



A₃V₂(PO₄)₃ (A = Na or Li) probed by *in situ* X-ray absorption spectroscopy

Maja Pivko ^{a,b}, Iztok Arcon ^{b,c,d}, Marjan Bele ^{a,b}, Robert Dominko ^{a,b,*}, Miran Gaberscik ^{a,b,e}

^a National Institute of Chemistry, Hajdrihova 19, SI-1000 Ljubljana, Slovenia

^b CO-NOT, Hajdrihova 19, SI-1000 Ljubljana, Slovenia

^c University of Nova Gorica, Vipavska 12, SI-5000 Nova Gorica, Slovenia

^d Jozef Stefan Institute, Jamova 39, SI-1000 Ljubljana, Slovenia

^e Faculty of Chemistry and Chemical Technology, University of Ljubljana, Askerceva 6, SI-1000 Ljubljana, Slovenia

HIGHLIGHTS

- *In situ* V XANES study in Li₃V₂(PO₄)₃ and Na₃V₂(PO₄)₃.
- *In situ* V EXAFS study in Li₃V₂(PO₄)₃ and Na₃V₂(PO₄)₃.
- Local environment of V atoms in NASICON structure during alkali metal deinsertion/insertion.

ARTICLE INFO

Article history:

Received 9 March 2012

Received in revised form

8 May 2012

Accepted 16 May 2012

Available online 23 May 2012

Keywords:

Li₃V₂(PO₄)₃

Na₃V₂(PO₄)₃

XAS

Li-ion batteries

Sodium batteries

NASICON

ABSTRACT

Two stable modifications of A₃V₂(PO₄)₃ (A = Na or Li) were synthesized by citric acid assisted modified sol–gel synthesis. The obtained samples were phase pure Li₃V₂(PO₄)₃ and Na₃V₂(PO₄)₃ materials embedded in a carbon matrix. The samples were tested as half cells against lithium or sodium metal. Both samples delivered about 90 mAh g^{−1} at a C/10 cycling rate. The change of vanadium oxidation state and changes in the local environment of redox center for both materials were probed by *in-situ* X-ray absorption spectroscopy. Oxidation state of vanadium was determined by energy shift of the absorption edge. The reversible change of valence from trivalent to tetravalent oxidation state was determined in the potential window used in our experiments. Small reversible changes in the interatomic distances due to the relaxation of the structure in the process of alkali metal extraction and insertion were observed. Local environment (vanadium–oxygen bond distances) after 1st cycle were found to be the same as in the starting material. Both structures have been found very rigid without significant changes during alkali metal extraction.

© 2012 Elsevier B.V. All rights reserved.

1. Introduction

Li-ion batteries not only play an important role in the progress of portable electronics but are also rapidly entering the segment of larger batteries designed for use in electric vehicles and in stationary applications [1]. The much broader use will increase the demand for lithium. As lithium ores are limited to a couple of countries, the pressure on prices will be high, the supply difficult to predict etc. [2]. Oppositely, sodium resources are inexhaustible and homogeneously spread around the globe. The sodium-ion battery (Na-ion) is expected to possess an energy density only a fraction lower compared to the lithium-ion counterpart. Thus, especially in

the large scale applications, where size is of secondary importance, Na-ion battery technology can represent an attractive alternative to Li-ion batteries.

Similarly to the Li-ion battery technology, also the Na-ion batteries will need to be studied in detail if we wish to understand the subtle modifications in structural properties and thus stability during the charge/discharge processes. In one part, we can proceed faster with the knowledge obtained during the extensive research of the Li-ion battery materials since some of the potentially useful materials can be prepared both as lithium or sodium analogs. One of them is the NASICON framework with a general chemical formula A₃V₂(PO₄)₃ where both lithium and sodium compositions can be used as cathode materials in Li-ion or Na-ion batteries [3–11]. The NASICON framework, known to possess inherently high ionic conductivity [3], is built of corner sharing VO₆ octahedra and PO₄ tetrahedra [7,12]. Li₃V₂(PO₄)₃ (denoted as LVP) exists in two crystallographic modifications, among them the

* Corresponding author. National Institute of Chemistry, Hajdrihova 19, SI-1000 Ljubljana, Slovenia. Tel.: +386 14760362; fax: +386 14760422.

E-mail address: Robert.Dominko@ki.si (R. Dominko).

monoclinic LVP form can be prepared via classical synthesis procedures [3] while the rhombohedral form LVP has been reported to be prepared by ion exchange of Na with Li [6] from the stable modification of sodium based structure (i.e. rhombohedral $\text{Na}_3\text{V}_2(\text{PO}_4)_3$ – denoted as NVP). Although the monoclinic and the rhombohedral forms of LVP exhibit different extraction/insertion mechanisms for lithium, both structures can exchange reversibly two lithium atoms in the voltage window between 3 and 4.2 V versus metallic lithium. Similar as rhombohedral LVP, also rhombohedral NVP can reversibly exchange sodium atoms from the structure. In general, the different insertion/deinsertion mechanism in monoclinic and rhombohedral analogs of $\text{A}_3\text{V}_2(\text{PO}_4)_3$ NASICON framework ($\text{A} = \text{Li}, \text{Na}$) can be observed as follows: the metal deinsertion from the monoclinic structure of $\text{A}_3\text{V}_2(\text{PO}_4)_3$ proceeds through several different two phase transitions [6] whereas the deinsertion from the rhombohedral modification proceeds only through one well established two-phase transition at 3.76 V for LVP [6] and 3.4 V for NVP [13].

Regardless of the mechanism of alkali metal exchange, one of the important parameters for long cycle life of active materials is the stability and reversible changes of the local environment of redox center.

Using in-situ X-ray diffraction it has been possible to understand the main mechanisms for both structures (monoclinic and rhombohedral) occurring during lithium extraction/insertion [6]. The same study has revealed the general structural stability (reversibility) during lithium extraction/insertion. However, to the best of our best knowledge there has been no study to probe changes in the local environment, more specifically, to find a correlation between the change of vanadium oxidation state and the quantity of extracted alkali metal.

The valence state of vanadium cations in the sample can be deduced from the energy shifts of the vanadium absorption edge [14,15]. A linear relation between the edge shift and the oxidation state was established for V atoms in different vanadium oxides: the absorption edge shifts for 2.5 eV per valence [14]. Different environments of the cation, most notably with different site symmetries, result in different K-edge profiles. In such cases, the comparison of the edge shifts may be hindered. However, when the sample contains the same cation in two different sites with different valence states and/or with different local structures, then the measured XANES spectrum is a linear combination of individual XANES spectra of the two cation sites. In such cases, a linear combination fit of the composed XANES spectrum with reference XANES spectra for each cation site can provide very precise information about the relative amounts of the cation in each valence state [15–17].

In this work, we focus on a comparative study of both stable modifications of the $\text{A}_3\text{V}_2(\text{PO}_4)_3$ framework ($\text{A} = \text{Li}, \text{Na}$) using in-situ X-Ray absorption spectroscopy. The aim of the work is to precisely monitor the respective vanadium oxidation states with V K-edge XANES and changes in the local environment of vanadium during first charge and discharge in both compounds with V K-edge EXAFS.

2. Experimental

LVP sample was prepared by using citric acid assisted modified sol–gel synthesis. Vanadium pentoxide (<99.6%, Aldrich) and citric acid (99%, Aldrich) in the ratio of 2:3 were dissolved in the demineralized water and mixed overnight. Stoichiometric amounts of lithium phosphate (99% Li_3PO_4 , Aldrich) and phosphoric acid (85% H_3PO_4 , Merck) were added to the obtained clear solution. Solvent was evaporated by rotary evaporator at 60 °C. The obtained

xerogel was further grinded and thermally treated under Ar atmosphere at 750 °C for 24 h. The heating rate was 10 °C min⁻¹.

The synthesis procedure of NVP sample was similar to the one described above, except that instead of Li_3PO_4 we used sodium hydroxide (99% NaOH, Merck) as a source for sodium.

The structural properties of the as prepared material were determined by X-Ray diffraction using a Bruker D5000 powder diffractometer with the $\text{CuK}\alpha$ radiation.

Electrodes for the electrochemical characterization, and electrodes for X-ray absorption spectroscopy (XAS) were prepared by ball-milling a mixture of active material, 10 wt.% of carbon black and 10 wt.% of EPDM (Ethylene-Propylene-Dien-Monomer Rubber) in cyclohexane. The obtained slurry was dried on 16 mm Al discs and the typical masses of active material were 5–6 mg (for standard electrochemical measurements) or 30–35 mg for *in-situ* XAS. The electrodes were left at 90 °C in vacuum during the night before use. A typical electrochemical cell consisted of two electrodes (working electrode and alkali metal counter electrode) which were separated with a Celgard® separator and vacuum-sealed in a triplex foil (coffee bag foil). The electrolyte was a 1 M solution of LiPF_6 in EC:DEC (1:1 ratio by volume) or 1 M solution of NaClO_4 in PC. The solvents were used as received and the salts were dried overnight at 90 °C in vacuum prior to use. The electrochemical characterization was performed on a VMP3 potentiostat/galvanostat at room temperature. *In-situ* electrochemical characterization was performed with an Autolab potentiostat/galvanostat using a C/15 cycling rate in the potential window: 2.4 V–4.2 V for LVP and 2.0–4.0 for NVP. The assembled batteries showed a total absorption thickness, μd , of about 2.5 above the vanadium K-edge. The spectra were recorded at room temperature in transmission mode at the XAFS beamline of the ELETTRA synchrotron radiation facility in Trieste, Italy. A Si (111) double crystal monochromator was used with about 0.7 eV resolution at V K-edge (5465 eV). Harmonics were eliminated by a slight detuning of the second monochromator crystal, keeping the intensity at 60% of the rocking curve. The intensity of the monochromatic X-ray beam was measured by three consecutive 30 cm long ionization detectors. The first was filled with 200 mbar N_2 and 1800 mbar He, the second with 1100 mbar N_2 and 900 mbar He, and third detector with 140 mbar Ar, 1000 mbar N_2 , and 860 mbar He.

The half battery was mounted on a sample holder between the first and the second ionization detector. The XAS spectra were measured initially on the as-prepared sample and repeated continuously during the first cycle. The measuring time for each spectrum was 29 min (in all, 35 XANES and EXAFS spectra were collected in the period of 1050 min for LVP and 27 spectra in the period of 880 min for NVP).

XAS spectrum of the reference V compound (V_2O_5) was measured on the homogeneous pellet with the total absorption thickness of about 2 above the V K-edge. V_2O_5 sample was prepared from micronised powder homogeneously mixed with micronised BN powder.

The absorption spectra were measured within the interval [-250 eV–1200 eV] relative to the V K-edge. In the XANES region equidistant energy steps of 0.25 eV were used, while for the EXAFS region equidistant k-steps ($\Delta k \approx 0.03 \text{ \AA}^{-1}$) were adopted with the integration time of 1 s/step. Exact energy calibration was established with the simultaneous absorption measurements on 5 micron thick V metal foil inserted between the second and third ionization cell. Absolute energy reproducibility of the measured spectra was ± 0.01 eV. The analyses of XANES and EXAFS spectra were performed with the IFEFFIT program package [18]. Model EXAFS spectra were constructed ab-initio with FEFF6 program code [19].

3. Results and discussion

X-ray diffraction patterns of the LVP and NVP samples used in this study are shown in Fig. 1a and b. The diffraction peaks in LVP correspond to the single phase of monoclinic $\text{Li}_3\text{V}_2(\text{PO}_4)_3$ crystallized in $P2_1/n$ space group [3], as shown in Fig. 1a. The diffraction peaks in NVP, however, correspond to rhombohedral $\text{Na}_3\text{V}_2(\text{PO}_4)_3$ crystallized in $R\bar{3}c$ space group [13], as shown in Fig. 1b. The content of carbon in as prepared composites was determined by thermogravimetric analysis (not shown) and it was found to be 12.6 wt.% and 6.8 wt.% in LVP and NVP sample, respectively.

Both samples were further electrochemically characterized by simple galvanostatic charge/discharge method. Fig. 2 shows charge/discharge curves for the LVP sample (Fig. 2a) and for the NVP sample (Fig. 2b), as well as the evolution of the discharge capacity in the first 20 cycles at a C/10 rate (Fig. 2c). LVP was cycled in the potential range between 3.0 V and 4.2 V vs. lithium reference. According to previous reports [5,20], in this potential range oxidation of V^{3+} into V^{4+} occurs through 3 well defined plateaus which have been explained by the two lithium atoms having non-equal positions in the structure. The reduction of vanadium into trivalent state is a reversible process; however we have observed an additional ill-defined plateau at approximately 3.8 V.

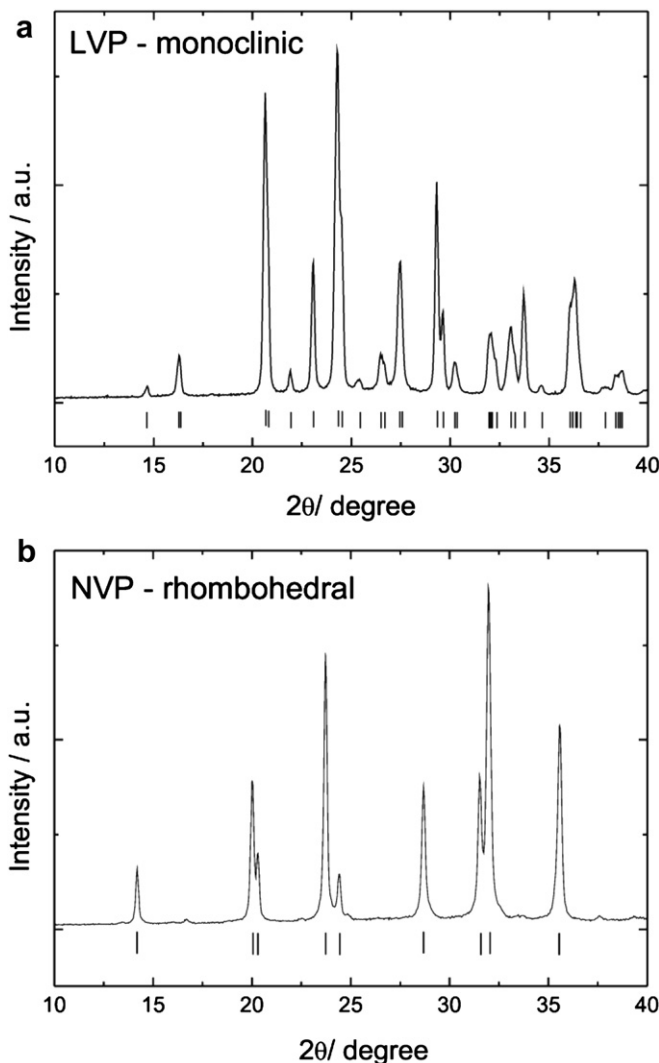


Fig. 1. XRD patterns of (a) LVP indexed with a monoclinic $P2_1/n$ space group and (b) NVP indexed with a rhombohedral $R\bar{3}c$ space group.

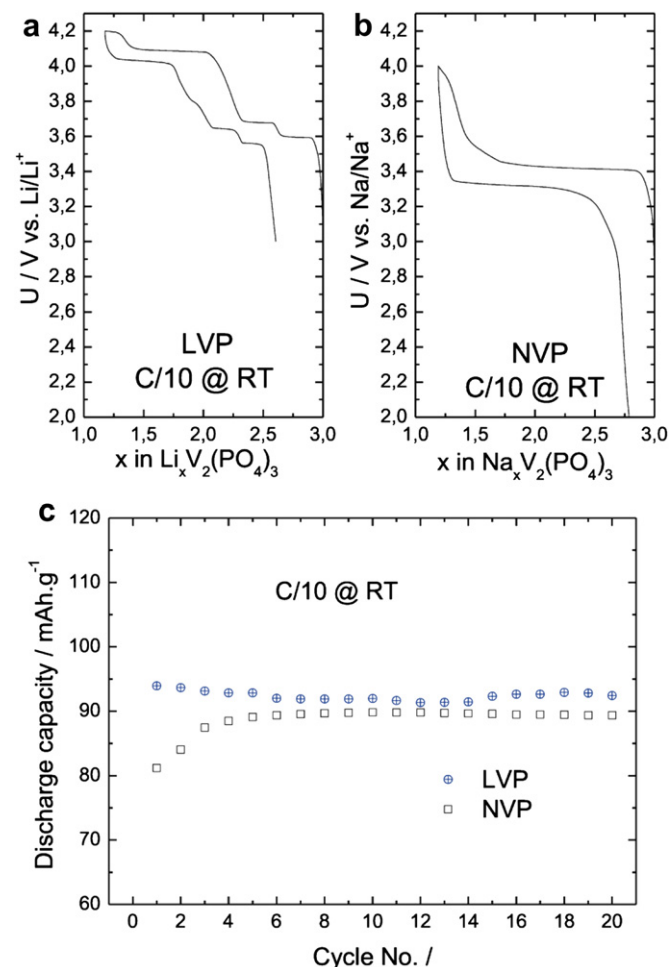


Fig. 2. a) first charge/discharge curves obtained at C/10 for LVP, b) first charge/discharge curves obtained at C/10 for NVP, and c) discharge capacity of both samples at C/10 in the first 20 cycles.

After stabilization in the first cycle, the cycling process revealed a constant capacity of slightly above 90 mAh g⁻¹. Since the thermodynamically stable modification of NVP is the rhombohedral structure, also the extraction mechanism is not expected to be the same as observed in LVP sample with the monoclinic structure. During the sodium extraction only one well defined plateau at 3.4 V was observed. The extraction of approximately 1.6 sodium atoms can be correlated to the change in oxidation state of vanadium from the trivalent close to the tetravalent oxidation state. The extraction process was reversible and after a few cycles the discharge capacity was stabilized close to the value of 90 mAh g⁻¹. The galvanostatic characterization confirmed a good quality of our samples, that is, appropriate for use in much more demanding *in situ* spectroscopy.

3.1. X-ray absorption spectroscopy

Changes in the vanadium valence state and local symmetry in LVP and NVP were monitored *in-situ* by vanadium K-edge XANES. Figs. 3 and 4 show the normalized V XANES spectra of LVP and NVP samples, respectively, during the oxidation and reduction in the first cycle. The spectra were normalized by a standard procedure [14,15]. In the pre-edge region all spectra exhibit very similar edge profiles with a weak triplet resonance structure, characteristic for octahedrally coordinated vanadium cations, lacking an inversion center [14].

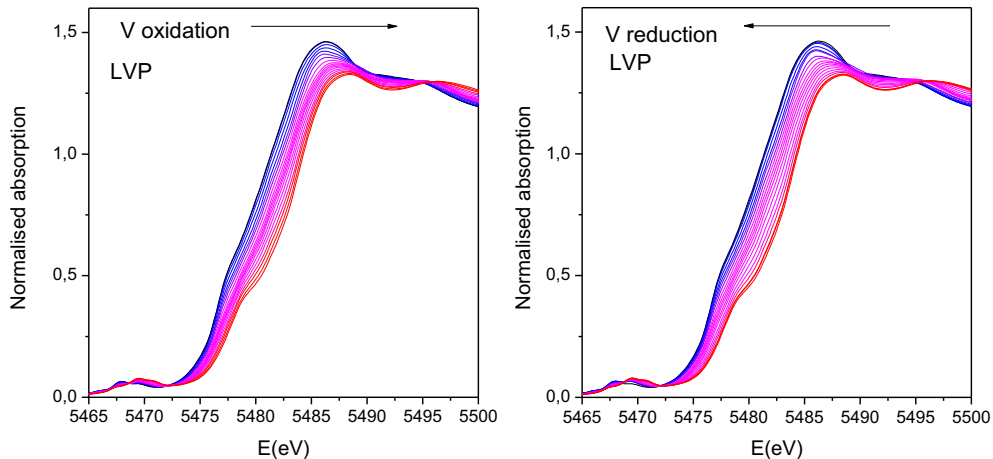


Fig. 3. The V K-edge XANES spectra of LVP during the oxidation and reduction in the first cycle.

The valence state of the V cation in the sample can be deduced from the energy shift of the absorption edge. With increasing oxidation state each absorption feature in the XANES spectrum is shifted to higher energies. The edge shifts of about 2.5 eV per unit valence were found in cases of different vanadium oxides [14].

For both cathode materials a shift of the V edge to higher energies is observed during battery charging (oxidation), indicating oxidation of vanadium, and in the process of discharging (reduction), gradual shifts of the edge to lower energies indicate the reduction of vanadium (Figs. 3 and 4). The edge position and shape after reduction is practically identical as that in the as-synthesized sample, which clearly indicates the complete reversibility of the changes in vanadium valence state and local structure during first cycle of charging/discharging.

The relative amounts of the vanadium in trivalent and tetravalent oxidation state can be precisely determined by a linear combination fit [15–18]. For both cathode materials the XANES spectra of intermediate states can be very well described by linear combinations of the XANES spectrum of the initial state of the battery, and the spectrum at the highest average vanadium oxidation state, obtained after complete charging. An example of the fit result for each material is illustrated in Fig. 5. In this way the relative amount of each component in all intermediate states was determined with a precision of 1% or better.

To deduce the average V valence state in the intermediate states the average V valence in both limiting states need to be determined

independently. For this purpose a comparison of the V edge energy with reference vanadium compounds with a similar composition and similar local symmetry of V atom neighborhood is used. The edge positions in as synthesized LVP and NVP samples are the same and coincide with that in reference Roscoelite and V_2O_3 [14,18], where vanadium is trivalent.

The average valence of V in the most oxidized state after charging is determined from the edge shift, relative to the edge position in the as synthesized sample. Taking into account the edge shift of 2.5 eV per valence, determined on reference vanadium oxides [14], we estimate the average valence of V in the most oxidized state of LVP and NVP samples after charging to be $V^{3.75+}$ and $V^{3.80+}$, respectively. The uncertainty in the determination of the average V valence of these two limiting states is about $\pm 5\%$.

The XANES results therefore show that during battery oxidation the average vanadium valence is gradually increased from $3.0+$ to $3.8+$. During reduction the average V valence gradually and reversibly decreases to its initial value of $V^{3.0+}$. The relative amount of V^{4+} valence state during the first cycle of charging and discharging of the LVP and the NVP battery is plotted in Fig. 6 (assuming that only V^{3+} and V^{4+} cations are present).

Expected monotonous change of oxidation with time was confirmed in both samples with a small perturbation within the LVP sample. Namely, a small shift in the slope occurred during the transition of the electrochemical curve from low voltage plateaus to the high voltage plateau (Fig. 6a). This can be explained by the two

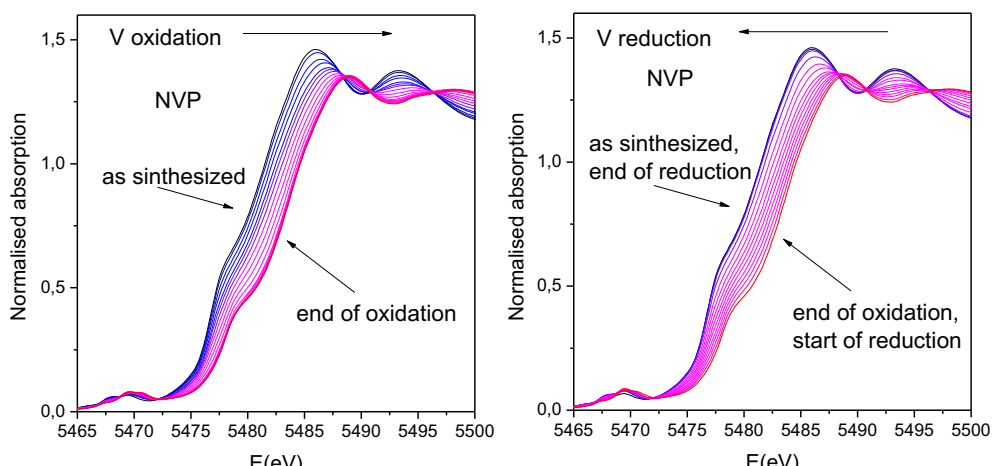


Fig. 4. The V K-edge XANES spectra of NVP during the oxidation and reduction in the first cycle.

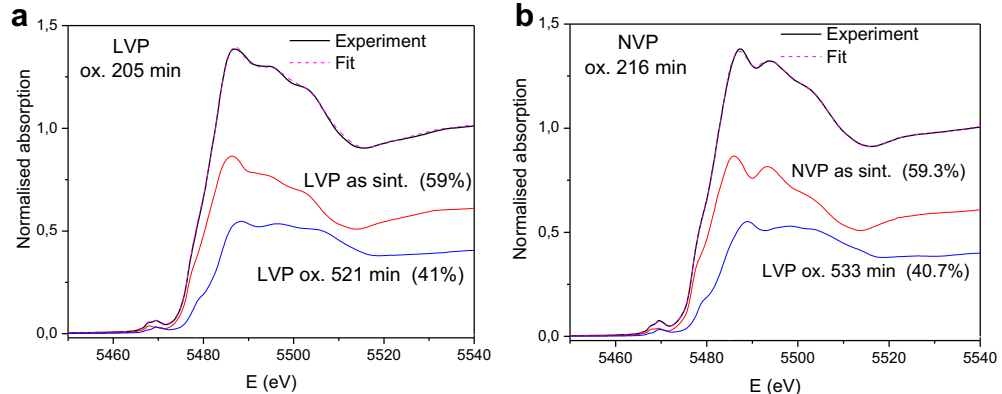


Fig. 5. (a) V K-edge XANES spectrum of LVP sample after 205 min of oxidation: Solid line - experiment; magenta dashed line - best-fit linear combination of XANES profiles of as prepared LVP sample ($V^{3.0+}$) and the spectrum at the highest average vanadium oxidation state, obtained after complete charging after 521 min of oxidation ($V^{3.75+}$) (both components are shown below). (b) V K-edge XANES spectrum of NVP sample after 216 min of oxidation: Solid line - experiment; magenta dashed line - best-fit linear combination of XANES profiles of as prepared NVP sample ($V^{3.0+}$) and the spectrum at the highest average vanadium oxidation state, obtained after complete charging after 533 min of oxidation ($V^{3.8+}$) (both components are shown below).

phase mechanism where a complete removal of lithium from one site should occur before the removal of a second lithium and the associated oxidation process can start [21]. In the present case, the observed nonlinear shift of oxidation state can partly be due to loose pressure on the electrode sandwich in the part that was in the beam focus surface area. Another important information observed

from Fig. 6 is a very slow or negligible change of the oxidation state at high voltages for both compositions.

Vanadium K edge EXAFS analysis is used to directly probe the changes in the short range order around vanadium cations in the LVP and NVP materials during oxidation and reduction. Fourier transforms of the representative EXAFS spectra from the series obtained during first charge/discharge cycle are shown in Fig. 7 and Fig. 8, revealing the contributions of individual shells of neighbor atoms around vanadium. A qualitative comparison showed that all the spectra in the series for both materials are very similar, indicating that the local environment around V cations in LVP and NVP

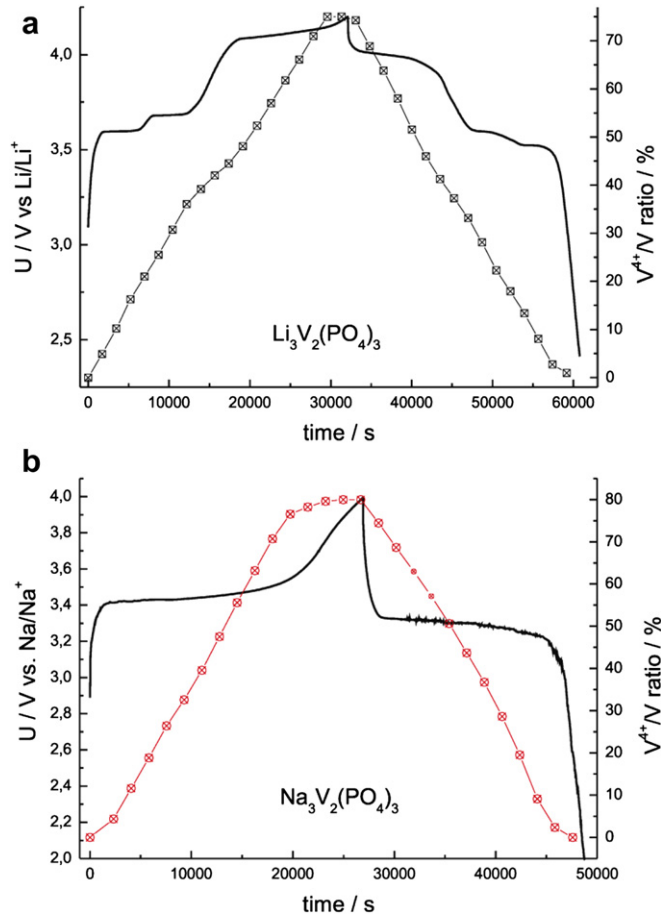


Fig. 6. The relative amount of V^{4+} component (right axis) during first cycle of charge/discharge as determined from V XANES in a) LVP sample and b) In NVP sample. Left y-axis shows the voltage profiles of the battery during the *in situ* measurements.

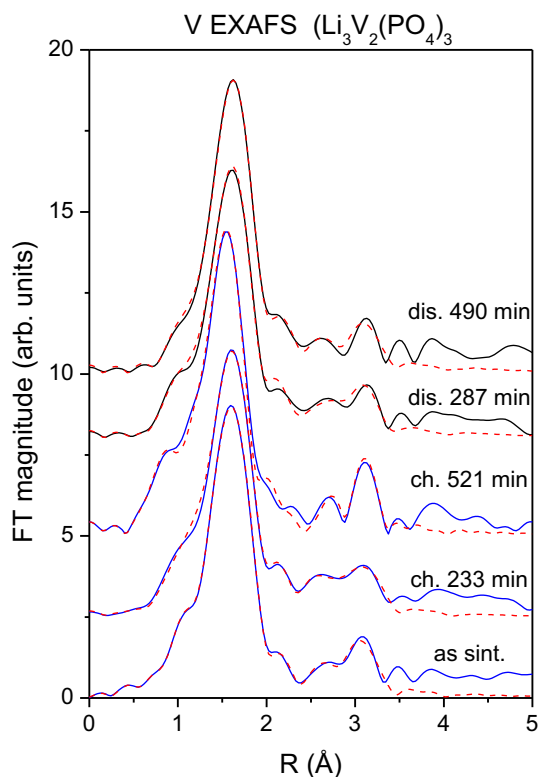


Fig. 7. Selected Fourier transform spectra of k^3 -weighted V EXAFS spectra of the LVP sample during the first cycle of charge and discharge. Experiment—solid line; EXAFS model—dashed line.

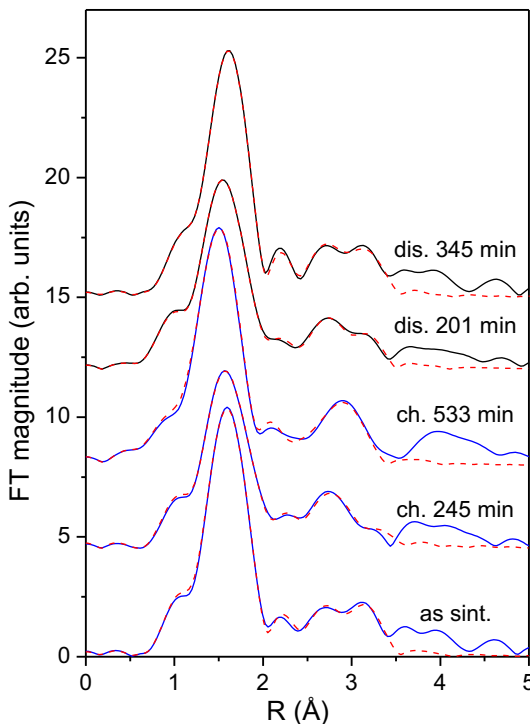


Fig. 8. Selected Fourier transform spectra of k^3 -weighted V EXAFS spectra of the NVP sample during the first cycle of charge and discharge. Experiment—solid line; EXAFS model—dashed line.

cathodes does not change significantly during the process of charging and discharging. Both structures are very rigid and stable, and after the first cycle they reversibly return to the structure of the as-prepared sample.

For the quantitative analysis we built the basic EXAFS model ab initio with FEFF6 program code [19], with the help of crystallographic data of as prepared LVP with $P2_1/n$ space group [8]. In this crystal structure V atoms occupy two crystallographic sites, at both they are octahedrally coordinated by six oxygen atoms. The V–O interatomic distances are distributed between 1.86 Å to 2.17 Å. More distant coordination shells in the R range up to 4 Å are composed of Li, P and O atoms.

The EXAFS model included six oxygen atoms in the first coordination shell, with two V–O scattering paths with different V–O distances. Three oxygen atoms were set at each distance, to describe the average deformation of the octahedron. Three scattering paths were used to describe the contribution of more distant coordination shells up to 3.5 Å: one containing Li neighbors and two composed of P atoms at two different distances.

Structural parameters were quantitatively resolved by comparing the measured signal with model signal in the best-fit procedure. For each scattering path the distance and Debye-Waller factor were varied, together with a common shift of energy origin ΔE_0 . The stoichiometry, however, was not varied: the degeneracy of individual scattering paths was fixed, except for the amount of Li atoms, which is adjusted to the extent of lithium extraction or insertion. The EXAFS amplitude reduction factor S_0^2 is kept fixed at the value of 0.90.

The model fits very well all the measured EXAFS spectra in the series in the k range of 3 Å⁻¹ to 14 Å⁻¹, and R range of 1 Å–3.3 Å. The quality of fit is illustrated in Fig. 7 on the selected (representative) spectra from the series measured during the first cycle of charging and discharging. Obtained structural parameters confirm that there are no significant changes of local structure during charging and discharging. In all cases the local structure around V is found to be

a deformed octahedron. In the initial (as prepared) state, the deformation is adequately described by three oxygen atoms at a distance of 1.96 ± 0.01 Å and three oxygen atoms at 2.06 ± 0.01 Å. During battery charging (oxidation of vanadium) both V–O distances are gradually decreased. In the most oxidized state after charging we found three oxygen atoms at 1.88 ± 0.01 Å and three oxygen atoms at 1.97 ± 0.01 Å. During battery discharging (reduction of vanadium) both V–O distances are gradually increased and reach the same values (within error bars) as in the as prepared sample. A common Debye-Waller factor (σ^2) of both V–O scattering paths gradually increases from 0.003 ± 0.01 Å² to 0.008 ± 0.03 Å² at the end of charging, indicating an increase in average static disorder, and returns to the initial value after discharging. There are no significant changes of local structure in more distant coordination spheres, except of small changes of interatomic distances due to the relaxation of the structure in the process of Li extraction and insertion.

Similar results were obtained in the EXAFS analysis of NVP sample. As in the case of LVP, the FEFF model, based on crystallographic data of as prepared NVP with $R\bar{3}c$ space group, included two V–O scattering paths with different V–O distances in the first coordination shell. Three oxygen atoms were set at each distance, to describe the average deformation of the octahedron. Three scattering paths were used to describe the contribution of more distant coordination shells up to 3.5 Å: one containing Na neighbors, one with O and one with P atoms. For each scattering path the distance and Debye-Waller factor were varied, together with a common shift of energy origin ΔE_0 . The degeneracy of individual scattering paths was fixed, except for the amount of Na atoms, which is adjusted to the extent of lithium extraction or insertion. The EXAFS amplitude reduction factor S_0^2 is kept fixed at the value of 0.90.

The model fits very well all the measured EXAFS spectra in the series in the k range of 3 Å⁻¹–12 Å⁻¹, and R range of 1.1–3.3 Å. The quality of fit is illustrated in Fig. 8 on the representative spectra from the series measured during the first cycle of charging and discharging.

Again, the only structural change that we found during battery charging/discharging, is the decrease of V–O interatomic distances in the first coordination sphere during charging. In as prepared state three oxygen atoms are at 1.95 ± 0.01 Å and three at 2.07 ± 0.01 Å. After charging we found three oxygen atoms at 1.86 ± 0.01 Å and three oxygen atoms at 1.97 ± 0.01 Å. During battery discharging both V–O distances are gradually increased and reach the same values (within error bars) as in the as prepared sample. A common Debye-Waller factor (σ^2) of both V–O scattering remains almost unchanged (0.004 ± 0.01 Å²) during charging and discharging. In more distant coordination spheres only small changes of interatomic distances are detected due to the relaxation of the structure in the process of extraction and insertion.

To conclude, the local structure around V atoms in both cathode materials is very rigid and does not change significantly in the process of lithium or sodium extraction and insertion. The analysis thus confirms structural stability and reversibility observed by in-situ XRD [6].

4. Conclusions

Both $\text{Li}_3\text{V}_2(\text{PO}_4)_3$ (LVP) and $\text{Na}_3\text{V}_2(\text{PO}_4)_3$ (NVP) materials synthesized by a citric assisted modified sol–gel process delivered a reversible capacity of about 90 mAh g⁻¹. The obtained capacity corresponds to the exchange of approximately 1.5 mol of Li in LVP and 1.6 mol of Na in NVP. This value is consistent with the results on average change of V oxidation state, obtained with in-situ XANES analysis. The average oxidation state of vanadium in the cathode changes from +3 to +3.75 in the case of LVP and from +3

to +3.8 in the case of NVP sample. The process is reversible, showing a high stability of used cathode materials. Vanadium K-edge EXAFS results, probing the local environment of V atoms *in situ*, revealed only small changes in the average bond length between vanadium and oxygen atoms in the first coordination sphere. The observed changes within the deformed oxygen octahedron are almost identical and reversible for both materials. To conclude, both cathode materials showed similar reversible structural deformations during alkali metal exchange which proves their rigidity and stability in both variations of high energy density batteries.

Acknowledgments

This work was supported by the Ministry of Education, Science and Sport of Slovenia, the Slovenian Research Agency (research programme P1-0112), and Center of Excellence Low-Carbon Technologies (CO NOT). Access to synchrotron radiation facilities of ELETTRA, Trieste, Italy beamline XAFS, project 20105073 is acknowledged. We thank Giuliana Aquilanti and Luca Olivi, from XAFS beamline at synchrotron ELETTRA for the support and expert advice on beamline operation.

References

- [1] M. Armand, J.-M. Tarascon, *Nature* 251 (2008) 652–657.
- [2] J.-M. Tarascon, *Nat. Chem.* 2 (2010) 510.
- [3] J. Gabuicher, C. Wurm, G. Goward, C. Masquelier, L. Nazar, *Chem. Mater.* 12 (2000) 3240–3242.
- [4] J. Gopalakrishnan, K.K. Rangan, *Chem. Mater.* 4 (1992) 745–747.
- [5] S.-C. Yin, H. Grondy, P. Strobel, H. Huang, L.F. Nazar, *J. Am. Chem. Soc.* 125 (2003) 326–327.
- [6] M. Morcrette, J.-B. Leriche, S. Patoux, C. Wurm, C. Masquelier, *Electrochem. Solid State Lett.* 6 (2003) A80–A84.
- [7] S.-C. Yin, P. Strobel, H. Grondy, L.F. Nazar, *Chem. Mater.* 16 (2004) 1456–1465.
- [8] S. Patoux, C. Wurm, M. Morcrette, G. Rousse, C. Masquelier, *J. Power Sources* 119–121 (2003) 278–284.
- [9] J. Barker, M.Y. Saidi, J.L. Swoyer, *Electrochem. Solid-State Lett.* 6 (2003) A53–A55.
- [10] A. Pan, J. Liu, J.-G. Zhang, W. Xu, G. Cao, Z. Nie, B.W. Arey, S. Liang, *Electrochem. Commun.* 12 (2010) 1647–1677.
- [11] Y. Uebou, T. Kiyabu, S. Okada, J.-i. Yamaki, *The Reports of Institute of Advanced Material Study*, 16, Kyushu University, (2002) 1–5.
- [12] I.V. Zatovsky, *Acta Cryst. E66* (2010) i12.
- [13] L.S. Plashnitsa, E. Kobayashi, Y. Noguchi, S. Okada, J.-i. Yamaki, *J. Electrochem. Soc.* 157 (2010) A536–A543.
- [14] J. Wong, F.W. Lytle, R.P. Messmer, D.H. Maylotte, *Phys. Rev. B* 30 (1984) 5596–5610.
- [15] R. Dominko, C.V.-A. Garrido, M. Bele, M. Kuezma, I. Arcon, M. Gaberscek, *J. Power Sources* 196 (2011) 6856–6862.
- [16] R. Dominko, I. Arcon, A. Kodre, D. Hanzel, M. Gaberscek, *J. Power Sources* 189 (2009) 51–58.
- [17] M. Kuezma, R. Dominko, D. Hanzel, A. Kodre, I. Arcon, T. Meden, M. Gaberscek, *J. Electrochem. Soc.* 156 (2009) A809–A816.
- [18] B. Ravel, M. Newville, *J. Synchrotron Radiat.* 12 (2005) 537.
- [19] J.J. Rehr, R.C. Albers, S.I. Zabinsky, *Phys. Rev. Lett.* 69 (1992) 3397–3400.
- [20] M.Y. Saidi, J. Barker, H. Huang, J.L. Swoyer, G. Adamson, *J. Power Sources* 119–121 (2003) 266–272.
- [21] W. Dreyer, J. Jamnik, C. Guhlke, R. Huth, J. Moškon, M. Gaberšček, *Nat. Mater.* 9 (2010) 448–453.